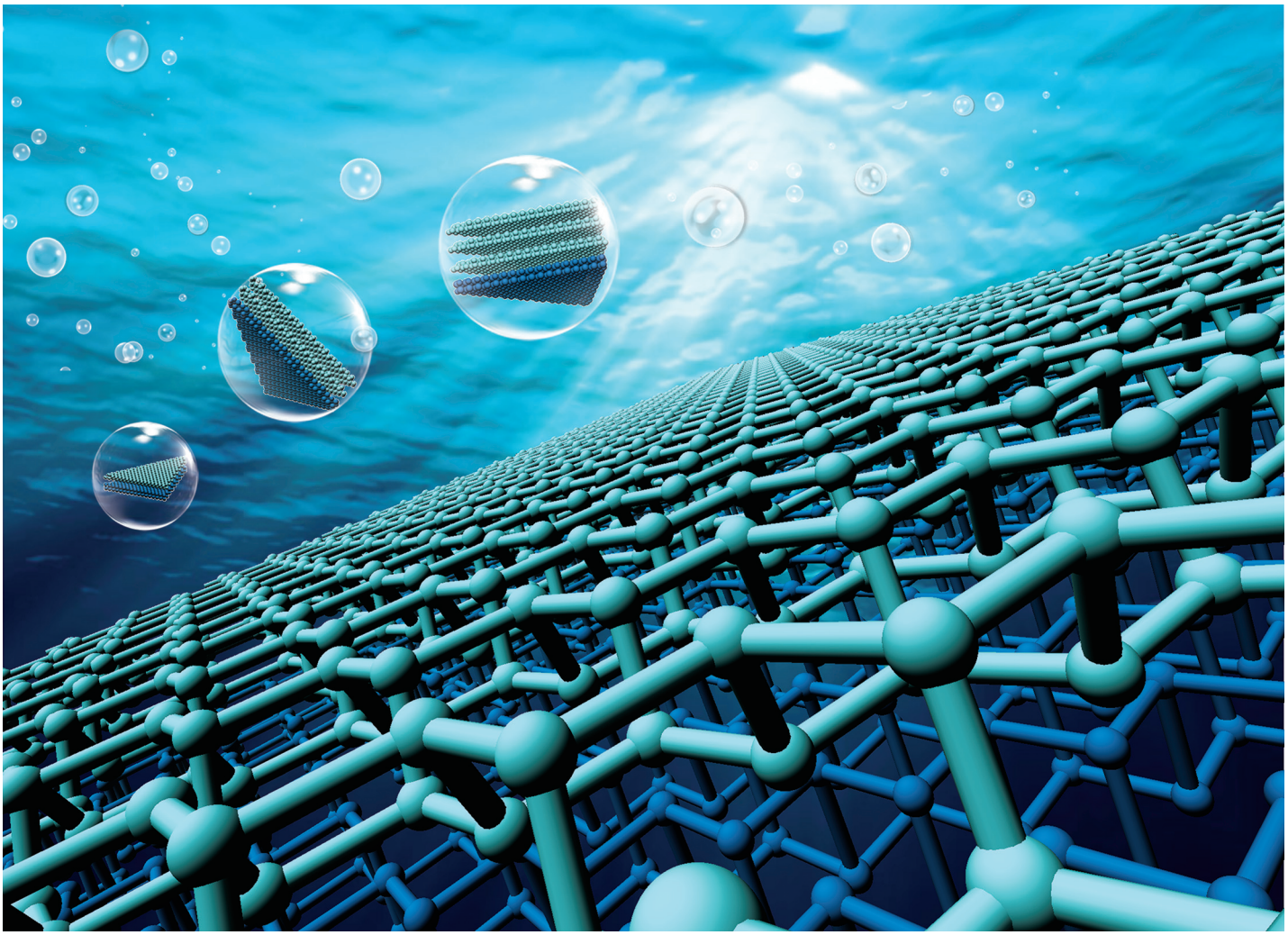

Showcasing research from Center for Nano Science and Technology, College of Chemistry and Material Science, The Key Laboratory of Functional Molecular Solids, Ministry of Education, Anhui Laboratory of Molecule-Based Materials, Anhui Normal University, Wuhu, China.

Layer-dependent electronic properties of phosphorene-like materials and phosphorene-based van der Waals heterostructures

Phosphorene has become an extremely fashionable 2D material in recent years. Isostructural to the phosphorene, however, MXs (M=Sn, Ge; X = S, Se) have received less attention. This work shows that van der Waals heterostructures with Moiré superstructures formed by mutual couplings among MXs and among MXs and few-layer phosphorene are able to show type-I or type-II characteristics and I-II or II-I transitions can be induced by adjusting the number of layers. As depicted in the illustration, our results are expected to create new opportunities for the design of novel optoelectronic and electronic devices, especially the applications of phosphorene-based heterostructures.

As featured in:

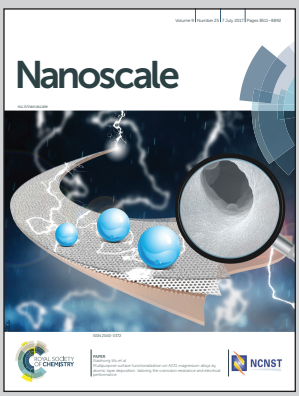

See Y. C. Huang *et al.*, *Nanoscale*, 2017, **9**, 8616.

ROYAL SOCIETY OF CHEMISTRY

rsc.li/nanoscale

Registered charity number: 207890

Nanoscale

PAPER

View Article Online
View Journal | View Issue

Cite this: *Nanoscale*, 2017, **9**, 8616

Layer-dependent electronic properties of phosphorene-like materials and phosphorene-based van der Waals heterostructures†

Y. C. Huang, * X. Chen, C. Wang, L. Peng, Q. Qian and S. F. Wang

Received 19th March 2017,
Accepted 26th April 2017

DOI: 10.1039/c7nr01952a

rsc.li/nanoscale

Black phosphorus is a layered semiconducting allotrope of phosphorus with high carrier mobility. Its monolayer form, phosphorene, is an extremely fashionable two-dimensional material which has promising potential in transistors, optoelectronics and electronics. However, phosphorene-like analogues, especially phosphorene-based heterostructures and their layer-controlled electronic properties, are rarely systematically investigated. In this paper, the layer-dependent structural and electronic properties of phosphorene-like materials, *i.e.*, mono- and few-layer MXs (M = Sn, Ge; X = S, Se), are first studied *via* first-principles calculations, and then the band edge position of these MXs as well as mono- and few-layer phosphorene are aligned. It is revealed that van der Waals heterostructures with a Moiré superstructure formed by mutual coupling among MXs and among MXs and few-layer phosphorene are able to show type-I or type-II characteristics and a I–II or II–I transition can be induced by adjusting the number of layers. Our work is expected to yield a new family of phosphorene-based semiconductor heterostructures with tunable electronic properties through altering the number of layers of the composite.

1. Introduction

As interesting and promising two-dimensional (2D) elemental materials, mono- and few-layer phosphorene could be isolated experimentally by mechanical or liquid exfoliation from its bulk form of black phosphorous.[1,2] It has been revealed that phosphorene has a tunable direct and layer-dependent band gap with a wide range from 0.3 of the bulk to 1.5 eV of the monolayer.[3,4] A high carrier mobility of up to 10^4 cm^2 V^{-1} s^{-1} and moderate on/off ratios of 10^4–10^5 were further reported, which are vital for semiconductor devices.[4–6] Furthermore, phosphorene has a negative Poisson rate,[7] excellent near-infrared properties and high photoelectric conversion capacity[8,9] as well as outstanding electrocatalytic performance toward the oxygen evolution reaction,[10] *etc.*, which leads to phosphorene having a huge potential and wide application. Although the research enthusiasm for phosphorene has not faded, phosphorene-like analogues have received less attention. As can be seen in Fig. 1a and b, MXs (M = Sn, Ge; X = S, Se) are isostructural to phosphorene, in which each M or X atom covalently bonds to three different neighboring atoms inside one MX layer, forming a puckered honeycomb network. Similar to graphite and other layered materials, the adjacent layers are held together by weak van der Waals interactions.[11,12] It is interesting that these MXs are isoelectronic counterparts to group V semiconductors, *e.g.*, the novel mono-elemental thin films 2D arsenene and antimonene proposed by Zhang *et al.*,[13,14] which are cousins of phosphorene. Motivated

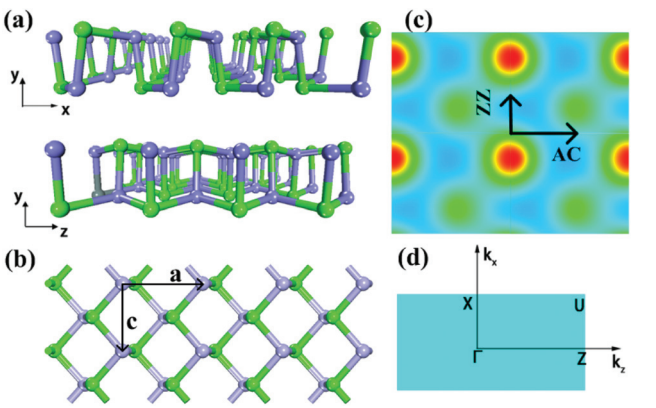

Fig. 1 Structural Illustration of MXs. (a) are side views along the *x*–*y* and *y*–*z* planes. The top view is shown in (b). The charge density distribution of the GeS monolayer is shown in (c) and the Brillouin zone is given in (d).

Center for Nano Science and Technology, College of Chemistry and Material Science, The Key Laboratory of Functional Molecular Solids, Ministry of Education, Anhui Laboratory of Molecule-Based Materials, Anhui Normal University, Wuhu, 241000, People's Republic of China. E-mail: huangyc@mail.ahnu.edu.cn

†Electronic supplementary information (ESI) available: Lattice parameters and band gaps of MXs bulk, layer-dependent band gaps of mono- and few-layer MXs, band gaps as the inverse number of layers and the construction of Moiré superstructures for SnSe/phosphorene heterostructure as well as the band structures of bulk, mono- and few-layer MXs. See DOI: 10.1039/c7nr01952a

by the fact that the properties of phosphorene are highly sensitive to its thickness, the layer-dependent properties of MXs have drawn great attention recently.[15–20] However, these studies either focused on one of the materials of this class, or no more than 5 layers were considered. In particular, the possible van der Waals heterostructures formed by MXs and isostructural phosphorene have still seldom been exploited. Note that van der Waals heterostructures are very crucial for the design of a new generation of novel nanodevices.[21]

In this paper, first-principles calculations are employed to systematically investigate the layer-dependent electronic properties of MXs of up to 5 layers. The band edge positions were aligned for both MXs and phosphorene. Many possible type-II alignments were found and a transition from type-II to I or type-I to II was predicted to be realizable by altering the number of layers. By construction of a Moiré superstructure of the SnSe/phosphorene heterostructure, we have proved that the inferences deduced from the band alignment calculations are reliable and powerful. This work opens a new branch of phosphorene-based heterostructures which is of great importance for applications in nanodevices.

2. Theoretical methods

In the present work, the numbers of layers of mono- and few-layer MXs are denoted by nL, n = 1 to 5. All the DFT calculations described in this work were performed using the projector augmented wave (PAW)[22] formalism, as implemented in the Vienna Ab initio Simulation Package (VASP).[23,24] The PBE exchange–correlation functional in the generalized gradient approximation (GGA)[25,26] was selected; the optB88[27] and DFT-D2[28,29] functions were also selected for comparison; and the cutoff energy for the plane-wave basis was set to 450 eV. An 8 × 3 × 8/5 × 1 × 5 k-point grid, as proposed by Monkhorst–Pack,[30] was used to sample the Brillouin zone for bulk/few-layer MXs structural optimizations. A finer 13 × 5 × 13/7 × 1 × 7 grid was employed for the electronic calculations. By minimizing the quantum mechanical stresses and forces, the lattice vectors and atomic positions were fully relaxed for all the considered structures. The convergence threshold was 10^{-5} eV for energy and 10^{-2} eV Å^{-1} for force. To remove spurious interactions between neighboring structures in periodic calculations, a vacuum layer of no less than 15 Å was constructed in the perpendicular direction. Spin-orbital coupling (SOC) is not considered because a previous investigation demonstrated that the bandgap differences with or without SOC are within 0.1 eV for MXs,[15] which is unlike the case of isoelectronic group V semiconductors of β-SbAs, where the SOC is significant (0.2 eV).[31] Such a small difference is insufficient to affect the band alignment prediction for the heterostructures. In addition, in order to give reliable results for the gap energies, we use a hybrid functional approximation of Heyd–Scuseria–Ernzerhof (HSE06)[32,33] for the exchange–correlation term because it is known to be underestimated when employing semilocal GGA approximations.

3. Results and discussion

We first optimized the lattice parameters of the bulk counterparts of all MXs. Three functionals, *i.e.*, PBE,[34] optB88[27] and DFT-D2,[29] are used and the obtained results are compared with the experimental ones. As can be seen in Table S1 (ESI†), the DFT-D2 results in which the weak dispersion interaction is included fit better with the experimental values, especially in the aspect of the layered direction. In Table S2,† we list the corresponding band gaps. All the calculated band gaps are underestimated, but the hybrid HSE06 functional[32,33] can correctly reproduce the experimental results (the band structures calculated by HSE06 are given in Fig. S1†). Therefore, the following band structures for mono- and few-layer MXs are calculated by the HSE06 functional starting with the relaxed structure at the DFT-D2 level.

In Table 1, we have tabulated the optimized lattice parameters of mono- and few-layer MXs. The available published data based on density functional theory (DFT) is also given for comparison. In general, the lengths of a and c are longer than their bulk counterparts because of the quantum confinement effect. Interestingly, with an increase in the number of layers, the length of a along the x-axis increases while the length of c along the y-axis slightly decreases. This scenario is consistent with the reported few-layer SnS,[20] which may be attributed to fact that the strength of bonding along the zigzag (c direction) is stronger than that along the armchair (a direction), such that the "a" direction receives more impact and the "c" direction suffers little perturbation. As exemplified in Fig. 1c, the charge density along the *ZZ* direction is obviously denser than that along the *AC* direction for the GeS monolayer. Note that GeS responds insensitively to the number of layers because it is the most compact among these MXs. These variation rules are quite consistent with recent experimental fabrications and theoretical phonon calculations for most group IV monochalcogenides.[35–37]

To check the stabilities of these layered MXs, we calculated the interlayer binding energies with the formula $E_b = (nE_1 - E_n)/(nA)$, where E_1 and E_n are the energies of the monolayer and n-layer systems, respectively and A is the surface area of the 2D unit cell. From Fig. 2a, it can be seen that with an increase in the numbers of layers, the binding energies increase and gradually approach their bulk limits. All the calculated binding energy values are comparable to or even larger than the corresponding ones of phosphorene, where the cleavage energy of an AB stacked bilayer is 16.6 ± 2.2 meV A^{-2}, and the bulk cleavage energy is 22.2 ± 1.6 meV A^{-2},[40] indicating that the MXs have a relatively higher stability.

Now we focus on the layer-dependent electronic properties of MXs. The Brillouin zone and the path along the desired high symmetry points are sketched in Fig. 1d. The band structures of each MX from 1 to 5 L (layer) are shown in Fig. S2–S5.† Since they have the same geometrical structure, all the band structure topologies are similar. The shape of the band dispersion around the Γ point along the Γ–X and Γ–Z branches is asymmetric, which indicates that there is an anisotropic be-

Table 1 Optimized lattice parameters of mono- and few-layer MXs at the DFT-D2 level. Comparisons with available published results are also given in brackets

	1 L		2 L		3 L		4 L		5 L	
	a	*c*	*a*	*c*	*a*	*C*	*A*	*c*	*a*	*c*
GeS	4.40	3.69	4.42	3.68	4.43	3.66	4.43	3.66	4.44	3.66
Ref. 38	(4.33)	(3.67)	(4.42)	(3.67)						
Ref. 15	(4.40)	(3.68)								
GeSe	4.28	3.99	4.32	3.98	4.37	3.97	4.39	3.95	4.39	3.97
Ref. 39	(4.24)	(3.94)	(4.31)	(3.97)						
Ref. 15	(4.26)	(3.99)								
SnS	4.23	4.07	4.27	4.07	4.38	4.04	4.40	4.04	4.41	4.03
Ref. 20	(4.31)	(4.04)	(4.34)	(4.02)	(4.34)	(4.02)	(4.36)	(4.02)	(4.38)	(4.00)
Ref. 15	(4.24)	(4.07)	(4.28)	(4.05)						
SnSe	4.36	4.30	4.43	4.25	4.49	4.24	4.50	4.24	4.52	4.22
Ref. 16, 37	(4.41)	(4.27)	(4.51)	(4.21)	(4.51)	(4.21)				
Ref. 15	(4.36)	(4.30)	(4.42)	(4.25)						

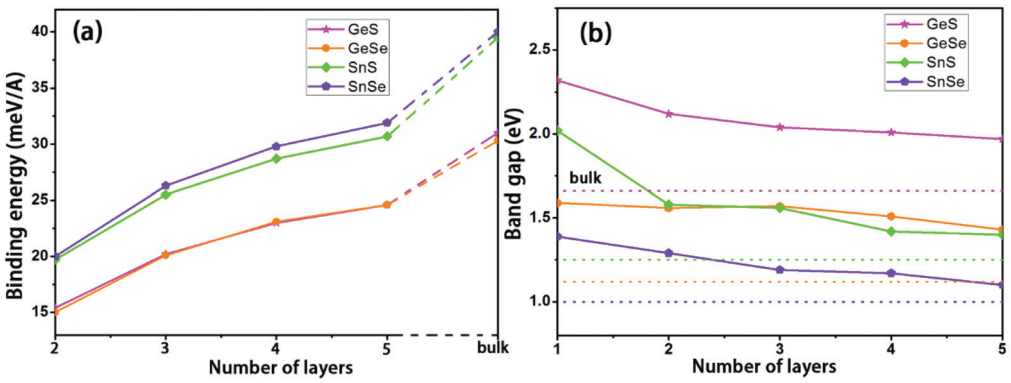

Fig. 2 Binding energies (a) and band gaps (b) of the layered MXs as a function of the number of layers.

havior of electronic structures for few-layer MXs, in agreement with previous investigations and that of phosphorene.[15,19,41]

The band gap variations at the HSE06 level are illustrated in Fig. 2b. As can be seen, the band gaps decrease and gradually approach their bulk limits with an increase in thickness. The strongest response to the number of layers is observed for SnS, but GeSe exhibits the weakest feedback. Except for GeSe, the largest decrease appears on the stage from 1 to 2 L. After 5 L stacking, the band gap has nearly converged with respect to the number of layers for SnS/SnSe, while that of GeS/GeSe has a relatively large deviation from the bulk and for which the gap is predicted to converge after more than 10 layers of packing. Because Se and S, Ge and Sn have essentially the same electronegativity, the lattice parameters of MXs are mostly determined by the ionic radius of the constituents and GeS, GeSe are thus the two most compact materials. Therefore, the slow convergent band gap of GeS/GeSe may result from the fact that the lattice parameters respond insensitively to the number of layers (Table 1).

To give and in-depth description of the relationship between band gap variation and the number of layers, we scale the band gap as the inverse number of layers in Fig. S6.† Good linear relationships are established (GeSe is excluded because of its insensitive response). The same situation is also found for phosphorene,[4] which embodies the quantum confinement effect. Of particular interest is that the band gap of phosphorene depends more sensitively on the number of layers, indicating that altering the number of layers may be an effective route to tuning the electronic property of phosphorene-based materials.

Fig. 3 shows the band alignment of the valence band maximum (VBM) and conduction band minimum (CBM) with respect to the vacuum level for 1 to 5 L based on the HSE06 calculations. Through the figure we can see that there is an obvious downward shift in CBM but a relatively insensitive response for VBM. In sharp contrast, the response of VBM to the number of layers is more sensitive than the response of CBM for phosphorene (Fig. 3, blue dotted lines). It is known that the energy difference between the valence/conduction band edge of a semiconductor and the work function of a metal determines the Schottky barrier height at the metal–semiconductor interface. Thus, the complementary responses

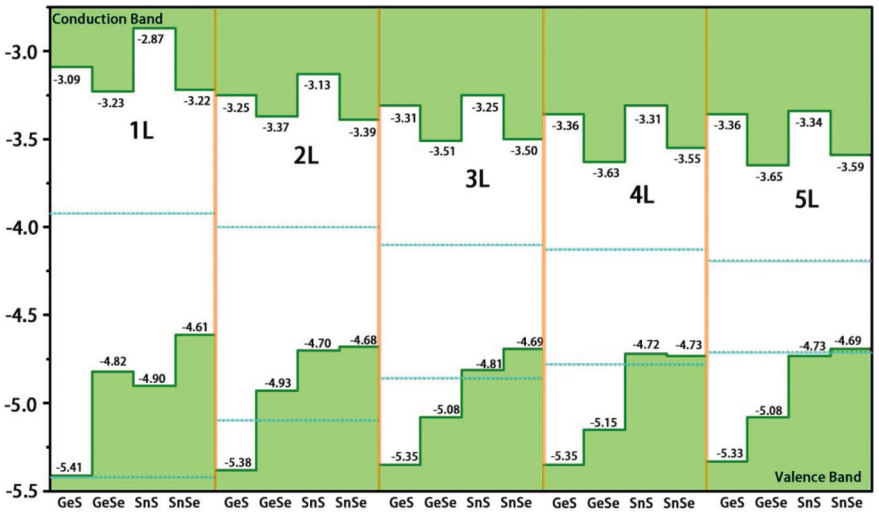

Fig. 3 Calculated band alignments of MXs from 1 to 5 L at the HSE06 level. The corresponding calculations for phosphorene are also shown as dotted blue lines for comparison. The vacuum level is taken as the zero reference.

of CBM in few-layer MXs and VBM in phosphorene as well as the strong layer-dependent edge position offers a practical way to modify the Schottky barrier height, which allows us to imagine more efficient electron/hole injection and electron/hole transport across the contact.

More importantly, the band alignment schematic shown in Fig. 3 can give abundant information for selectively choosing type-II heterostructures. In this type of alignment, the electrons and holes are completely separated, resulting in a decrease in the recombination rate of carriers, which is favored in electronics, photovoltaics, optoelectronics, and photocatalysis. It can be seen that only GeS and SnS with the same layers can form the type-II alignment. But with a consideration of the band edge position of phosphorene, many type-II candidates are present. For example, both the CBM and VBM of 1 L-phosphorene have lower energies than the corresponding band edge states of other 1 L-MXs. This type-II behavior disappears for GeS/phosphorene with both components having two layers, but lasts up to 5 layers for SnSe/phosphorene, 4 layers for SnS/phosphorene and 2 layers for GeSe/phosphorene. Interestingly, altering the numbers of a one-constituent layer can lead to a transition from type-II to I or type-I to II. Especially for phosphorene, the band edge position (blue horizontal dotted lines in Fig. 3) is highly sensitive to the number of layers, which provides a golden opportunity for artificial modulation of the electronic properties of the MXs/phosphorene heterostructures. A representative example is 1 L GeSe/phosphorene: natively it has a typical type-II alignment; however, when there are more than 4 phosphorene layers, they can transform into type-I. The tunable band alignment in the heterostructures greatly interests us, so that we chose 1 L-SnSe coupled with different layers of phosphorene to investigate the layer-dependent electronic properties as well as the role of the band alignment.

Because of the large lattice mismatch, we constructed the rotated Moiré superstructure[21,42,43] for the SnSe/phosphorene heterostructure with the lattice deformations of both materials minimized, as illustrated in Fig. 4. In this model, the lattice misfit is only 0.1% and the mismatch angle is 12.3°. Note that using the lattice match model in which the two layers are manually stretched or compressed, so as to make the base vectors of one lattice identical to those of another lattice, always falsely describes the interface structures and the properties of the van der Waals heterostructure.[44] In fact, such a weak binding energy between two layers makes it hard to achieve the formation of the common lattice.[45] To check the stacking stabilities, we calculated the heterostructure formation energies by subtracting the energy summation of the two independent materials from the total energies of the heterostructure, and the obtained results are −168, −88, −59, −43 and −35 meV per P atom for 1 to 5 L phosphorene/SnSe, respectively. The relatively low and negative values demonstrate that they are energetically stable.

We first align the band edge positions of SnSe and few-layer phosphorene in Fig. 5a. It can obviously be seen that with the increase in the number of layers, the CBM energy of phosphorene decreases and is always lower than that of SnSe, while the VBM energy increases and gradually approaches that of SnSe, such that the type-II characteristic gets somewhat fuzzy because of the greater and greater hybridization between SnSe and P to produce the VBM of the heterostructure. To check the tendency of a type-II to type-I transition with the variation in the number of phosphorene layers, we further studied their electronic structures by using the HSE06 method. The band structures of each heterostructure are shown in Fig. 5b–f, respectively, where the blue/red dotted lines indicate the proportional contribution from P/SnSe (Fig. 5g). First, the calculated band gaps are 0.566, 0.560, 0.480, 0.461 and 0.445 eV for SnSe/nL-phosphorene (n = 1, 2, 3, 4 and 5), respectively. The variation trend agrees perfectly with the prediction from band alignment calculations and the band

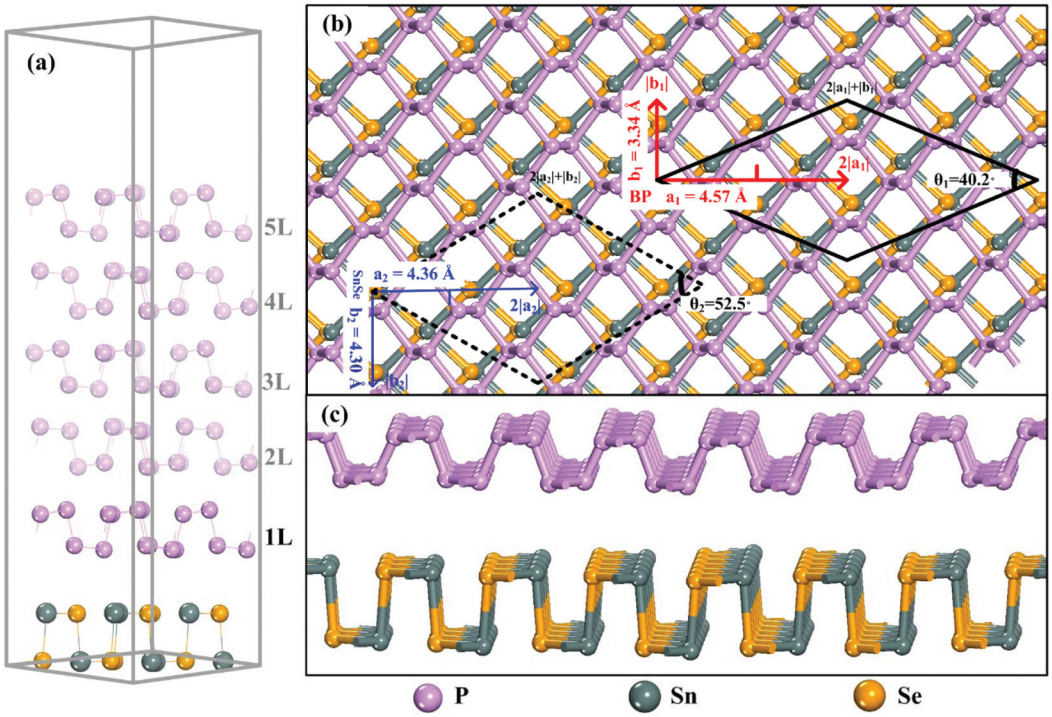

Fig. 4 (a) Model of SnSe/phosphorene heterostructures with Moiré superstructures. One to five layers of phosphorene are considered. Top view (b) and side view (c) of schematic representations of 1 L phosphorene on the SnSe substrate. The model construction details can be seen in the ESI.†

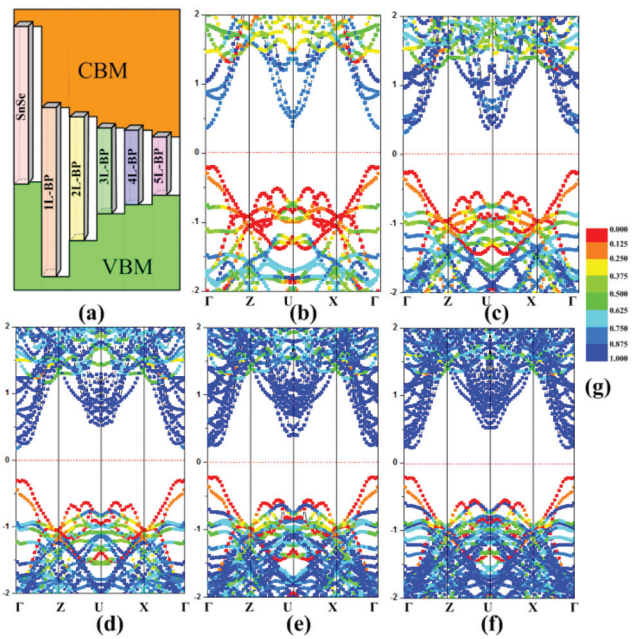

Fig. 5 (a) Band alignment of SnSe monolayer and few-layer phosphorene. (b)–(f) are the band structures of SnSe coupled with 1 to 5 L phosphorene, respectively. The color bar is shown in (g).

gap magnitudes are quite close to the energy difference between the lowest point of the conduction band and the highest point of the valence band in the band alignment diagram. Second, from 1 to 5 L, because the CBM energy difference between SnSe and phosphorene increases, the contribution from P to the heterostructure CBM gradually increases from 78 to 100%. On the other hand, the contribution from the P and SnSe mixture to the VBM increases, which is a result of the VBM energy difference between SnSe and phosphorene decreasing. It was found that the contribution from SnSe to the VBM decreases from 100 to 76% when 5 L-phosphorene is coupled with a SnSe monolayer. Note that the band gap of 5 L-phosphorene is 0.58 eV, which is still much higher than that of its bulk counterpart (0.39 eV by HSE06). Thus, it is expected that with a further increase in the number of phosphorene layers, the VBM energy of phosphorene may exceed that of SnSe, leading to a heterostructure displaying a type-I characteristic. Different types of alignment would cause different carrier confinement effects; both are useful but have different applications. The controllable electronic properties would provide a possible new way to tune the carrier localization in a SnSe/phosphorene heterostructure, which would be useful to improve the performance of nanoscale optoelectronic devices.

The above investigation on SnSe/phosphorene perfectly demonstrated that the calculation of the band alignment is able to correctly forecast the electronic properties of the heterostructure. The power of the band alignment shown in Fig. 3 not only suggests the possible carrier localization when two materials form a van der Waals heterostructure, but also gives a visual reference for constructing the desired devices by tuning the number of one of the layers in the material. Therefore, on one hand, a new class of heterostructures, such

as the mutual coupling of the MXs or phosphorene/MX systems, which are expected to raise great investigation interest in the science community, is founded. On the other hand, the layer-dependent electronic properties of MXs and phosphorene provide new ideas for the design of novel optoelectronic devices. For example, similar to the sensitive electronic property of phosphorene, the VBM of GeSe and the CBM of SnS also respond strongly to the number of layers. Since little investigation on phosphorene-based heterostructures has been reported, our results will greatly enrich the research fields on phosphorene and phosphorene-like materials and point to a new avenue for designing optoelectronic devices.

4. Conclusions

In conclusion, we have systematically studied the layer-dependent structural and electronic properties of phosphorene-like material MXs (M = Sn, Ge; X = S, Se). It was observed that in general 2D-MXs have longer lattice parameters than their bulk counterparts, due to the quantum confinement effect. With an increase in the number of layers, the band gaps of the MXs gradually decrease and approach the bulk limits. Band alignment calculations showed that van der Waals heterostructures formed by mutual coupling among MXs and among MXs and few-layer phosphorene are predicted to manifest versatile electronic properties, *i.e.*, type-I and type-II alignments as well as the layer-dependent I–II or II–I transitions. By construction of a lattice mismatch model, the rotated Moiré superstructure of SnSe/phosphorene was chosen as an example for this series of heterostructures to explore the layer-dependent electronic properties and to verify the predictions from band alignment calculations. The calculated magnitude and variation of band gaps are indeed in line with the results deduced from the band alignment. The tendency from type-II to type-I was also confirmed when SnSe is coupled with phosphorene with an increase in the number of layers of phosphorene. Our results are expected to create new opportunities for the design of novel optoelectronic and electronic devices, especially the applications of phosphorene-based heterostructures.

Acknowledgements

This work was supported by National Natural Science Foundation of China no. 21573002 (H. Y.) and 21373012 (W. S.). The numerical calculations in this paper have been done on the super-computing system in the Supercomputing Center of University of Science and Technology of China.

Notes and references

1 L. Li, Y. Yu, G. J. Ye, Q. Ge, X. Ou, H. Wu, D. Feng, X. H. Chen and Y. Zhang, *Nat. Nanotechnol.*, 2014, **9**, 372–377.
2 H. Guo, N. Lu, J. Dai, X. Wu and X. C. Zeng, *J. Phys. Chem. C*, 2014, **118**, 14051–14059.
3 H. O. H. Churchill and P. Jarillo-Herrero, *Nat. Nanotechnol.*, 2014, **9**, 330.
4 H. Liu, A. T. Neal, Z. Zhu, X. Xu, D. Tomanek, P. D. Ye and Z. Luo, *ACS Nano*, 2014, **8**, 4033–4041.
5 J. Qiao, X. Kong, Z.-X. Hu, F. Yang and W. Ji, *Nat. Commun.*, 2014, **5**, 4475.
6 J. Jia, S. K. Jang, S. Lai, J. Xu, Y. J. Choi, J.-H. Park and S. Lee, *ACS Nano*, 2015, **9**, 8729–8736.
7 J.-W. Jiang and H. S. Park, arXiv preprint arXiv:1403.4326, 2014.
8 T. Low, A. Rodin, A. Carvalho, Y. Jiang, H. Wang, F. Xia and A. C. Neto, *Phys. Rev. B: Condens. Matter*, 2014, **90**, 075434.
9 F. Xia, H. Wang and Y. Jia, *Nat. Commun.*, 2014, **5**, 4458.
10 B. Sa, Y.-L. Li, J. Qi, R. Ahuja and Z. Sun, *J. Phys. Chem. C*, 2014, **118**, 26560–26568.
11 S. Narita, Y. Akahama, Y. Tsukiyama, K. Muro, S. Mori, S. Endo, M. Taniguchi, M. Seki, S. Suga and A. Mikuni, *Physica B*, 1983, **117**, 422–424.
12 Y. Maruyama, S. Suzuki, K. Kobayashi and S. Tanuma, *Physica B*, 1981, **105**, 99–102.
13 J. Ji, X. Song, J. Liu, Z. Yan, C. Huo, S. Zhang, M. Su, L. Liao, W. Wang, Z. Ni, Y. Hao and H. Zeng, *Nat. Commun.*, 2016, **7**, 13352.
14 S. Zhang, Z. Yan, Y. Li, Z. Chen and H. Zeng, *Angew. Chem., Int. Ed.*, 2015, **54**, 3112–3115.
15 L. C. Gomes and A. Carvalho, *Phys. Rev. B: Condens. Matter*, 2015, **92**, 085406.
16 A. K. Deb and V. Kumar, *Phys. Status Solidi B*, 2017, **254**, 1600379.
17 L. Huang, F. Wu and J. Li, *J. Chem. Phys.*, 2016, **144**, 114708.
18 G. Shi and E. Kioupakis, *Nano Lett.*, 2015, **15**, 6926–6931.
19 G. A. Tritsaris, B. D. Malone and E. Kaxiras, *J. Appl. Phys.*, 2013, **113**, 233507.
20 C. Xin, J. Zheng, Y. Su, S. Li, B. Zhang, Y. Feng and F. Pan, *J. Phys. Chem. C*, 2016, **120**, 22663–22669.
21 A. K. Geim and I. V. Grigorieva, *Nature*, 2013, **499**, 419–425.
22 P. E. Blöchl, *Phys. Rev. B: Condens. Matter*, 1994, **50**, 17953.
23 G. Kresse and J. Hafner, *Phys. Rev. B: Condens. Matter*, 1993, **47**, 558.
24 J. P. Perdew and W. Yue, *Phys. Rev. B: Condens. Matter*, 1986, **33**, 8800.
25 Y. Zhang and W. Yang, *Phys. Rev. Lett.*, 1998, **80**, 890.
26 J. Klimeš, D. R. Bowler and A. Michaelides, *J. Phys.: Condens. Matter*, 2009, **22**, 022201.
27 A. D. Becke, *Phys. Rev. A*, 1988, **38**, 3098.
28 Q. Peng, G. Wang, G.-R. Liu and S. De, *Phys. Chem. Chem. Phys.*, 2014, **16**, 19972–19983.
29 S. Grimme, *J. Comput. Chem.*, 2006, **27**, 1787–1799.
30 H. J. Monkhorst and J. D. Pack, *Phys. Rev. B: Solid State*, 1976, **13**, 5188.
31 S. Zhang, M. Xie, B. Cai, H. Zhang, Y. Ma, Z. Chen, Z. Zhu, Z. Hu and H. Zeng, *Phys. Rev. B: Condens. Matter*, 2016, **93**, 245303.

32 J. Heyd, J. E. Peralta, G. E. Scuseria and R. L. Martin, *J. Chem. Phys.*, 2005, **123**, 174101.
33 J. Heyd, G. E. Scuseria and M. Ernzerhof, *J. Chem. Phys.*, 2003, **118**, 8207–8215.
34 J. P. Perdew, K. Burke and M. Ernzerhof, *Phys. Rev. Lett.*, 1996, **77**, 3865.
35 L. Li, Z. Chen, Y. Hu, X. Wang, T. Zhang, W. Chen and Q. Wang, *J. Am. Chem. Soc.*, 2013, **135**, 1213–1216.
36 R. Fei, W. Li, J. Li and L. Yang, *Appl. Phys. Lett.*, 2015, **107**, 173104.
37 L.-C. Zhang, G. Qin, W.-Z. Fang, H.-J. Cui, Q.-R. Zheng, Q.-B. Yan and G. Su, arXiv preprint arXiv:1505.04590, 2015.
38 F. Li, X. Liu, Y. Wang and Y. Li, *J. Mater. Chem. C*, 2016, **4**, 2155–2159.
39 S. Zhang, S. Liu, S. Huang, B. Cai, M. Xie, L. Qu, Y. Zou, Z. Hu, X. Yu and H. Zeng, *Sci. China Mater.*, 2015, **58**, 929–935.
40 L. Shulenburger, A. D. Baczewski, Z. Zhu, J. Guan and D. Tomanek, *Nano Lett.*, 2015, **15**, 8170–8175.
41 Y. Cai, G. Zhang and Y. W. Zhang, *Sci. Rep.*, 2014, **4**, 6677.
42 B. Hunt, J. D. Sanchez-Yamagishi, A. F. Young, M. Yankowitz, B. J. LeRoy, K. Watanabe, T. Taniguchi, P. Moon, M. Koshino and P. Jarillo-Herrero, *Science*, 2013, **340**, 1427–1430.
43 H. Fang, C. Battaglia, C. Carraro, S. Nemsak, B. Ozdol, J. S. Kang, H. A. Bechtel, S. B. Desai, F. Kronast and A. A. Unal, *Proc. Natl. Acad. Sci. U. S. A.*, 2014, **111**, 6198–6202.
44 X. Zhao, L. Li and M. Zhao, *J. Phys.: Condens. Matter*, 2014, **26**, 095002.
45 J. Kang, J. Li, S.-S. Li, J.-B. Xia and L.-W. Wang, *Nano Lett.*, 2013, **13**, 5485–5490.